ELSEVIER

Contents lists available at ScienceDirect

Journal of Molecular Liquids

journal homepage: www.elsevier.com/locate/mollig





COSMO-RS predictive screening of type 5 hydrophobic deep eutectic solvents for selective platform chemicals absorption

Thomas Quaid, Toufiq Reza

Department of Biomedical and Chemical Engineering and Sciences, Florida Institute of Technology, 150 West University Boulevard, Melbourne, FL 32901, United States

ARTICLE INFO

Keywords:
Deep Eutectic Solvents
Platform Chemicals
Separation
COSMO
Sigma potential
Excess enthalpy

ABSTRACT

Platform chemicals are crucial to the development of designer chemicals in industry; however, the utilization of these chemicals is limited from requiring separation from an aqueous phase. Type 5 hydrophobic deep eutectic solvents (HDES) have recently proven their ability to extract various low concentration solutes from aqueous solution. However, identifying a suitable HDES experimentally is a daunting task due to the large number of hydrogen bond donors (HBD), hydrogen bond acceptors (HBA), and their mixing ratio, with the HDES being ever increasing. In this study, Conductor-like Screening MOdel for Real Solvents (COSMO-RS) was utilized for over one hundred HDES and their relative solubilization ability for sorbitol, 5-hydroxymethyl furfural, and levulinic acid. Moreover, energetic mechanisms of solubilization were analyzed through the prediction of sigma profiles, sigma potentials, activity coefficients, and excess enthalpy of absorption. COSMO-RS results show that HBAs with tetra alkyl chains and amino acid-based HBDs are suitable HDES components for absorbing sorbitol, 5-hydroxymethyl furfural, and levulinic acid through a combination of van der Waals and hydrogen bonding interactions. These interactions are quantitatively examined through calculated excess enthalpy predictions, for example tetrabutylammonium bromide and arginine with a compositional ratio of 8:1, respectively, had an excess enthalpy of mixing with HMF of -7.9 kcal/mol despite the steric hindrance factor valuing ~ 4.0 kcal/mol.

1. Introduction

Platform chemicals (PCs) are used by chemical and manufacturing industries everyday products [1]. Among hundreds of potential PCs, U.S. Department of Energy has identified twelve most prominent ones namely sorbitol, xylitol, ethanol, furfural, 5-hydroxymethyl furfural (HMF), glycerol, isoprene, succinic acid, 2,5-furandicarboxylic acid, 3-hydroxypropionic acid, lactic acid, and levulinic acid [1–3]. In general, these PCs can be categorized as sugars, furans, and acids. Many of the PCs are sustainably synthesized from biomass using biological, biochemical, and thermochemical pathways [1,4]. However, these PCs are usually in the aqueous phase and sustainable separation of PCs has been challenging as thermal separation is often not viable [4,5].

Deep Eutectic Solvents (DES) are a relatively new class of green solvents defined by their composition of two or more chemicals which, when added together, incur a significant eutectic point depression [6]. These parts are categorized as being hydrogen bond acceptor (HBA) and hydrogen bond donor (HBD). For example, HBA like choline chloride (melting point, $T_m \sim 302~{}^{\circ}\text{C}$) and HBD like urea ($T_m \sim 133~{}^{\circ}\text{C}$) in a

mixture of 1:2 M ratio form DES with a melting point of 12 °C [7,8]. Among the four types of DES, only type 3 DESs are considered as environmentally benign and are generally cheaper alternatives to conventional solvents used in the industry [9-11]. However, due to the hydrogen bonding capabilities, most of the earlier studied type 3 DES (e. g., choline chloride-urea) have proven to be hydrophilic [12]. To date the bulk of applications for the solvents have been studied for nonpolar liquid and gaseous systems, where hydrophilic DES are preferable for separation [13-16]. However, separation of solutes like PCs from aqueous phase requires a hydrophobic DES. Hence, a separate class of DES (type 5) has been introduced as hydrophobic deep eutectic solvents (HDES) [17]. Table 1 shows a wide range of HDES reported in the literature. HBDs often have significant impacts on hydrophobicity of HDES, even when paired with hydrophilic HBAs [18]. Currently most commonly used HBA for HDES are menthol and thymol [19]. However, these two HBAs exhibit very different hydrogen bond properties in an HDES combination. Menthol possesses a high capacity to accept protons and thymol has a high capacity to donate protons [20]. Moreover, adjusting the alkyl chain lengths of the tetra-alkyl ammonium based-

E-mail address: treza@fit.edu (T. Reza).

^{*} Corresponding author.

 Table 1

 HDES studied in this project along with predicted densities, compositions, abbreviations, and literature sources.

No	Abbreviation	НВА	НВО	Ratio/REF	Density g/ml
1	N4Br AA	Tetrabutylammonium Chloride	acetic acid	1:1 [43]	1.031
2	N4Br HA	Tetrabutylammonium Chloride	hexanoic acid	1:2 [43]	0.988
3	N4Br CcA	Tetrabutylammonium Chloride	caprylic acid	1:2 [43]	0.971
4	N4Br CA	Tetrabutylammonium Chloride	decanoic acid	1:2 [16]	0.959
5	N4Br LA	Tetrabutylammonium Chloride	lauric acid	1:2 [44]	0.971
6	N4Br GA	Tetrabutylammonium Chloride	L-glutamic acid	6:1 [45]	1.044
7	N4Br P	Tetrabutylammonium Chloride	L-proline	4:1 [18]	1.037
8	N4Br A	Tetrabutylammonium Chloride	L-arginine	8:1 [18]	1.035
9	N4Br Bol	Tetrabutylammonium Chloride	1-butanol	1:1 [46]	0.973
10	N4Br Ool	Tetrabutylammonium Chloride	1-octanol	1:1 [46]	0.956
11	N4Br Lol	Tetrabutylammonium Chloride	lauryl alcohol	1:1 [46]	0.942
12	N4Br Oleyl	Tetrabutylammonium Chloride	oleyl alcohol	1:1 [46]	0.929
13	MTOA_Cl HA	Methyltrioctylammonium Chloride	hexanoic acid	1:2 [47]	0.892
14	MTOA_Cl CcA	Methyltrioctylammonium Chloride	caprylic acid	1:2 [47]	0.887
15	MTOA Cl CA	Methyltrioctylammonium Chloride	decanoic acid	1:2 [47]	0.883
16	MTOA_Cl LA	Methyltrioctylammonium Chloride	lauric acid	1:2 [47]	0.880
17	MTOA_Cl MA	Methyltrioctylammonium Chloride	myristic acid	1:1 [47]	0.874
18	MTOA_Cl PA	Methyltrioctylammonium Chloride	palmitic acid	1:1 [47]	0.863
			-		
19	MTOA_Cl OlA	Methyltrioctylammonium Chloride	oleic acid	1:2 [47]	0.878
20	MTOA_Cl RA	Methyltrioctylammonium Chloride	ricinoleic acid	1:2 [47]	0.903
21	MTOA_Cl Pol	Methyltrioctylammonium Chloride	N-propanol	1:2 [47]	0.847
22	MTOA_Cl Bol	Methyltrioctylammonium Chloride	1-butanol	1:2 [47]	0.846
23	MTOA_Cl Hol	Methyltrioctylammonium Chloride	hexanol	1:2 [47]	0.846
24	MTOA_Cl Ool	Methyltrioctylammonium Chloride	1-octanol	1:2 [46]	0.847
25	MTOA_Cl Dol	Methyltrioctylammonium Chloride	1-decanol	1:2 [46]	0.855
26	MTOA_Cl Lol	Methyltrioctylammonium Chloride	lauryl alcohol	1:2 [20]	0.847
27	MTOA_Cl Mol	Methyltrioctylammonium Chloride	myristyl alcohol	1:1 [20]	0.853
28	MTOA_Cl C	Methyltrioctylammonium Chloride	cetyl alcohol	1:2 [20]	0.847
29	MTOA_Cl Col	Methyltrioctylammonium Chloride	cyclohexanol	1:2 [20]	0.891
30	MTOA Cl Mol	Methyltrioctylammonium Chloride	DL-menthol	1:2 [20]	0.873
31	MTOA_Cl EG	Methyltrioctylammonium Chloride	ethylene glycol	1:2 [48]	0.905
32	MTOA_Cl PDol	Methyltrioctylammonium Chloride	propanediol	1:2 [48]	0.932
33					0.943
	MTOA_Cl Gly	Methyltrioctylammonium Chloride	glycerol	1:2 [48]	
34	MTOA_Cl BD	Methyltrioctylammonium Chloride	1,4-butanediol	1:2 [48]	0.896
35	MTOA_Cl TD	Methyltrioctylammonium Chloride	tetradecanol	1:2 [48]	0.847
36	MTOA_Cl HQ	Methyltrioctylammonium Chloride	hydroquinone	1:1 [49]	0.929
37	MTOA_Cl PP	Methyltrioctylammonium Chloride	p-phenylphenol	1:1 [49]	0.930
38	MTOA_Cl CP	Methyltrioctylammonium Chloride	4-cyanophenol	1:2 [49]	0.964
39	MTOA_Cl EP	Methyltrioctylammonium Chloride	ethylparaben	1:2 [50]	0.986
40	MTOA_Cl PAA	Methyltrioctylammonium Chloride	PhenylAcetic_Acid	1:3 [46]	0.943
41	N8Br PD	Tetraoctylammonium chloride	pentanediol	1:3 [51]	0.948
42	N8Br CA	Tetraoctylammonium chloride	decanoic acid	1:2 [17]	0.925
43	N8Br HA	Tetraoctylammonium chloride	hexanoic acid	1:2 [52]	0.939
44	N8Br EG	Tetraoctylammonium chloride	ethylene glycol	1:3 [51]	0.967
45	TOPO DHTU	Trioctylphosphine Oxide	dihexylthiourea	1:2 [53]	0.940
46	TOPO DD	Trioctylphosphine Oxide	decanediol	1:1 [53]	0.885
47	TOPO DTBC	Trioctylphosphine Oxide	ditertbutylcatechol	1:2 [53]	0.922
			-		
48	TOPO BZ	Trioctylphosphine Oxide	cyclohexylidenebisphenol	1:2 [53]	1.024
49	TOPO Ph	Trioctylphosphine Oxide	phenol	1:2 [53]	0.930
50	Menthol FA	Menthol	formic acid	1:1 [54]	0.930
51	Menthol AA	Menthol	acetic acid	1:1 [55]	0.925
52	Menthol LaA	Menthol	DL-lactic acid	1:1 [56]	0.978
53	Menthol CcA	Menthol	caprylic acid	1:1 [56]	0.899
54	Menthol CA	Menthol	decanoic acid	1:1 [56]	0.894
55	Menthol CA2	Menthol	capric acid	1:2 [57]	0.897
56	Menthol LA	Menthol	lauric acid	3:1 [57]	0.886
57	Menthol PA	Menthol	palmitic acid	4:1 [20]	0.882
58	Menthol PyA	Menthol	pyruvic acid	1:2 [43]	1.025
59	Menthol LaA	Menthol	DL-lactic acid	1:2 [58]	1.029
60	Menthol LevA	Menthol	levulinic acid	1:1 [59]	0.975
61	Menthol AyA	Menthol	acrylic acid	1:2 [58]	0.953
62	Menthol PrpA	Menthol	propionic acid	1:2 [58]	0.938
63	Menthol ByA	Menthol	butyric acid	1:2 [58]	0.926
			-		
64	Menthol VA	Menthol	valeric acid	1:2 [58]	0.921
65	Menthol HA	Menthol	hexanoic acid	1:1 [43]	0.906
66	Menthol CcA	Menthol	caprylic acid	1:2 [44]	0.905
67	Menthol CA	Menthol	decanoic acid	1:2 [60]	0.897
68	Menthol LA	Menthol	lauric acid	2:1 [61]	0.887
69	Menthol OlA	Menthol	oleic acid	1:2 [58]	0.886
70	Menthol K	Menthol	ketoprofen	1:2 [62]	1.096
71	Menthol DcF	Menthol	diclofenac	1:2 [62]	1.204
			phenyl salicylate		1.053

(continued on next page)

HBAs impacts polarity, where longer chains result in less polar solvents [21].

Similar to the HBA, changing the chain length on HBDs can affect the polarity of the HDES [22]. There are several examples of alkyl chain HBDs like butanoic acids to dodecanoic acids and butanol to dodecanol. Another effect of alkyl chain length is steric hindrance. Through an increase in steric hindrance via chain length on HBA and/or HBD, van Osch *et al* [17] discovered a positive correlation between hydrophobicity and a negative correlation between length and solute uptake. The density of HDES is also affected by alkyl chain length which can influence ease of separation from liquid-liquid systems applications [23]. Deng *et al* [24] found that with high density solvents, phase separation becomes more pronounced in liquid-liquid equilibrium dispersion extraction methods.

Inspired by literature, it can be hypothesized that HDES could be used to extract PCs from water. However, due to the nearly limitless combinations of HBA and HBD in varying compositions and binary/ternary configurations, experimental determinations of HDES for extraction of PCs are challenging. A Conductor-like Screening MOdel for Real Solvents (COSMO-RS) screening procedure could be a viable option to understand the desirable absorption characteristics of HDES for PC absorption. COSMO-RS utilizes density functional theory (DFT) to create non-empirical *ab initio* predictions. COSMO-RS relies on DFT constructed molecular energy structures, then applies exact statistical thermodynamics for evaluating the molecular interactions [25].

Jiriste et. al. [26] and Adeyemi et al [27] have proven suitability for two computational analytical methods including COSMO-RS in their predictive power for DES and ionic liquid (IL) systems reporting error for DES systems of \sim 8% regarding enthalpy of mixing predictions and < 10% error in HDES liquid–liquid system extraction predictions respectively. COSMO-RS was used in those studies due to its superior flexibility and screening potential over other conventional computational methods. In addition, a study by Canada-Barcala et al [28] was

performed using terpene based HDES with the common platform chemical furfural, the results of which showed superior performance by HDES over the two conventional solvents of toluene and methyl isobutyl ketone (MIBK) with HDES reported extraction yields of 90.6% and furfural selectivity over water at up to 75.3%. This research also performed an error analysis between COSMO-RS predicted results and experimental results which produced an R^2 value greater than 0.86 in all cases. Another study by McGaughy et al [12] regarding furfural extraction with HDES reported extraction yields up to 85% molar in tetrahexylammonium bromide with acid HBD. This research also reported errors between COSMO-RS and Experimental literature of less than 5%. However, to the best of authors knowledge, there is little to no research done with the use of COSMO-RS for the studied PC extraction by HDES. Therefore, a COSMO-RS screening of HDES was performed in this study to determine appropriate electrostatic characteristics of HDES (surface charge distributions) that is required for the efficient absorption of PCs like sorbitol, HMF, and levulinic acid. The characteristics of solvation were further studied through sigma potentials, sigma profiles, activity coefficients, and excess enthalpy contributions.

2. COSMO-RS simulation

The three PCs studied here are sorbitol, HMF, and levulinic acid which represent three main groups of identified PCs of sugars, furans, and acids, respectively. For HDES, 105 combinations of HDES were used for this study (Table 1). COSMO-RS thermodynamic property predictions were performed over several steps in computational sequences. First, all available molecule files for selected PCs and HDES components (HBAs and HBDs) were compiled from the extended COSMO-RS database. The HBA and HBD that were not available in the database (e.g., [N4Br]) were then imported from PubChem in the SMILES format. If the HBA and HBD are not available in PubChem, the molecules were drawn on the 3D molecule builder in TmoleX (version 4.5.3 N). For the latter

Table 1 (continued)

No	Abbreviation	НВА	HBD	Ratio/REF	Density g/ml
73	Menthol Ldc	Menthol	lidocaine	2:1 [63]	0.913
74	Menthol Myol	Menthol	myristyl alcohol	2:1 [63]	0.860
75	Menthol Nap	Menthol	napthol	2:1 [63]	0.953
76	Menthol PA	Menthol	palmitic acid	2:1 [20]	0.882
77	Menthol Cam	Menthol	camphor	1:1 [64]	0.913
78	Menthol TD	Menthol	tetradecanol	2:1 [63]	0.860
79	Thymol CA	Thymol	decanoic acid	1:1 [65]	0.927
80	Thymol LevA	Thymol	levulinic acid	1:1 [66]	1.026
81	Thymol LA	Thymol	lauric acid	1:2 [20]	0.909
82	Thymol MA	Thymol	myristic acid	2:1 [20]	0.926
83	Thymol PA	Thymol	palmitic acid	2:1 [20]	0.942
84	Thymol SA	Thymol	stearic acid	4:1 [20]	0.930
85	Thymol Cou	Thymol	coumarin	1:1 [63]	1.083
86	Thymol Mol	Thymol	L-(-)-menthol	1:1 [63]	0.917
87	Thymol Cam	Thymol	camphor	1:1 [65]	0.951
88	Thymol UA	Thymol	10-undecenoic acid	1:1 [65]	0.910
89	Thymol Bo	Thymol	borneol	1:1 [64]	0.942
90	Thymol So	Thymol	sobrerol	7:3 [64]	0.971
91	Thymol Be	Thymol	betaine	3:1 [18]	0.985
92	Lauric acid CcA	Lauric acid	caprylic acid	1:3 [67]	0.909
93	Lauric acid NA	Lauric acid	pelargonic acid	1:3 [67]	0.905
94	Lauric acid CA	Lauric acid	decanoic acid	1:2 [67]	0.900
95	Lauric acid L	Lauric acid	lidocaine	2:1 [40]	0.916
96	Lauric acid At	Lauric acid	atropine	2:1 [40]	0.977
97	Lauric acid Psy	Lauric acid	phenyl salicylate	1:1 [40]	1.039
98	Carvacrol LvA	Carvacrol	levulinic acid	1:1 [66]	0.997
99	Lipotril DA	Lipotril	decanoic acid	1:2 [68]	0.953
100	Lipotril Pyol	Lipotril	phenethyl alcohol	1:4 [69]	1.029
101	HFIP Be	Hexaflouroisopropanol	betaine	2:1 [24]	1.439
102	HFIP Car	Hexaflouroisopropanol	(-)-L-carnitine	2:1 [24]	1.409
103	Betaine PAA	Betaine	phenylacetic acid	1:2 [18]	1.134
104	Betaine Gya	Betaine	glycolic acid	1:2 [18]	1.236
105	Atropine DA	Atropine	decanoic acid	1:2 [40]	0.996

two methods, the individual HBAs and HBDs were solved for their lowest energy geometrical configurations in TmoleX. At this point, the sigma surfaces are generated for the molecules in addition to the geometrical configuration. All DFT calculations were performed at the basis point density functional theory b-p DFT level and Karlsruhe (Ahlrichs) def2-TZVP (default-2 Valence Triple-Zeta Polarization) basis set as recommended by TmoleX [29]. When applicable, the HBA were treated as ion pairs within the same TmoleX input file. Next, the optimized geometries of each molecule were sent to COSMOConf18 to test and generate geometrical conformers and sigma surfaces for each molecule. Finally, the conformer files for each molecule are uploaded to COSMO-RS where they are energetically averaged and used in the prediction of all studied thermodynamic properties (excess enthalpy and activity coefficient) and physical properties (e.g., density). Eq. (1) was used to express solvent-solute chemical potentials of HDES and platform chemicals by COSMO-RS after the energetic contribution terms are solved for misfit energy (E_{misfit}), hydrogen bond energy (E_{HB}), and van der Waals energy (E_{vdw}).

$$\mu_{s}(\sigma) = -\frac{RT}{a_{eff}} \ln \left[\int p_{s}(\sigma') e^{\left(\frac{a_{eff}}{RT} \left(\mu_{s}(\sigma') - E_{misfit}(\sigma, \sigma') - E_{HB}(\sigma, \sigma')\right)\right)} d\sigma' \right]$$
 (1)

where $\mu_s(\sigma)$ is the potential of a system to a surface of polarity (σ) . The σ and σ' are two interacting surface segments between two molecules. Meanwhile, a_{eff} is the effective contact area, which is used to account for geometric artifacts and misfits in the interacting molecular surfaces. E_{misfit} accounts for the energies associated with the geometrically nonideal contact and E_{HB} represents the electrostatics associated with hydrogen bonding. $p_s(\sigma)$ is the distribution function or sigma profile. R is the ideal gas constant and T is absorption temperature.

Next the calculated sigma potentials were used to determine the chemical potential of compound i in the HDES (S). This is achieved through Eq. (2) where the potential of the system is integrated over the surface of the compounds. C is a designated combinatorial term that accounts for area and volume geometric characteristics of differing molecules.

$$\mu_S^i = \mu_{C,S}^i + \int p^i(\sigma)\mu(\sigma)d\sigma \tag{2}$$

At this point using the chemical potentials thermodynamic parameters like Gibbs free energy, enthalpy, and activity coefficients were calculated. The activity coefficient of PCs in HDES (γ_S^i) was calculated through the difference of the chemical potential of PC i in HDES (μ_S^i) and the chemical potential of the PC in its pure form (μ_i^i) . This is achieved through Eq. (3).

$$\gamma_{sol}^{\infty,i} = exp(\mu_s^i - \mu^i)/RT) \tag{3}$$

The excess enthalpy of a system was solved through Eq. (4). Where H_{int} is the excess enthalpy of mixing or excess enthalpy of interaction for each molecule in the system, $H_{i,mix}$ and $H_{i,pure}$ are the enthalpies of the molecule i in the mixture and in pure form respectively. x_i is the composition of component i.

$$H_{int} = \sum_{i} x_i (H_{i,mix} - H_{i,pure}) \tag{4}$$

In COSMO-RS, the sigma values from Eq. (1) were used to calculate the misfit enthalpy (H_m) , hydrogen bonding enthalpy (H_{hb}) , and van der Waals enthalpy (H_{vdw}) . The purpose of this was to allow for differing contribution factors for each type of enthalpy as they have varying influences per system. The excess enthalpy of interaction (H_{int}) is the summation of these categories as seen in Eq. (5).

$$H_{int} = H_{mf} + H_{hb} + H_{vdw} \tag{5}$$

3. Results and discussion

3.1. COSMO-RS validation

Due to COSMO-RS being an ab-initio tool, it can be considered a powerful resource for screening HDES in various applications. However, the simulation might need validation with literature. The significance of this validation could confirm the molecular modeling done through TmoleX regarding the geometrical and electronic surface configurations, and the accuracy of these calculations affects the accuracy of all successive thermodynamic parameter estimations. In this study, the applicability of COSMO-RS simulations to model HDES was confirmed by predicting densities of HDES and compared with literature. Table S1 showed densities of 72 HDES solvents that are predicted by COSMO-RS and compared with literature values. Fig. 1 depicts the calculated densities of HDES, which are compared with experimental values from literature. It is apparent that the COSMO-RS predictions are slightly overestimated in general, but still show strong agreement with literature. The associated deviation is likely due to the overestimation of hydrogen bonding occurring between the HBA and HBD, causing overall higher molecular packing. An analysis on COSMO-RS predictions regarding DES was performed by Coutinho et al [30] who found overestimations of excess enthalpy produced by hydrogen bonding between the DES components. Regardless, the associated error is expected to have minimal impact due to the low standard deviation (<2%) results of experimental values from the average of the literature values. This conclusion is also supported by the findings of other research groups who have also used COSMO-RS to analyze HDES systems. For example, Adevemi et al [27] used COSMO-RS to evaluate chlorophenol extraction from water using HDES and reported good agreement between computational and experimental results. Wang et al [31] concluded that COSMO-RS is accurate and reliable for the use of DES and HDES in the extraction of pesticides from water. Jelinski et al [32] found strong correlation between experimental and computational activity coefficients for the solubilization of rutin by DES. Meanwhile, Darwish et al [33] compared COSMO-RS results with experimental for the use of HDES to extract aromatics from diesel and found an average Root Mean Square Deviation (RMSD) of 3.71.

3.2. Sigma surfaces, sigma profiles, and sigma potentials of sorbitol, HMF, and levulinic acid and HDES

Fig. 2 shows the computed sigma surfaces of sorbitol, HMF, and levulinic acid. Sigma surface is a visual representation of the energy signatures calculated by TmoleX after the geometric optimizations. The colors of the cloud around the ball and stick molecule structure represent sigma surface charge. The colors range from blue, to green, to red, which represent charge deficiency, charge neutrality, and charge density, respectively. The sigma surface is divided into geometrical segments. The segments are called sigma values, and the associated charges as sigma potentials [34]. The sigma values can be evaluated to learn about the mechanisms of molecular system interactions through analyzing sigma profiles and sigma potential plots [35,36]. Owing to the wide charge distribution in each PC (as seen in Fig. 3a), it is clear that there will be complex relationships developed between HDES and these solutes. For example, the limit of charge deficient sigma value (negative direction) for levulinic acid is $-0.023 e/\text{Å}^2$ and the limit of charge dense sigma (positive direction) is $0.018 e/\text{Å}^2$, which would be represented by the most saturated blue and red in Fig. 2, respectively. For HMF, the sigma range is $-0.02~e/\text{\AA}^2$ and $0.018~e/\text{\AA}^2$, whereas sorbitol contains sigma values between $-0.021 e/\mathring{A}^2$ and $0.02 e/\mathring{A}^2$. Each of these PC's contain nearly identical electrostatic surface charge ranges (x-axis). This is likely due to their stable organic nature, which limits them from extending into the radical regions $(e/\sigma > 0.03e/\text{Å}^2; \sigma < -0.03e/\text{Å}^2)$

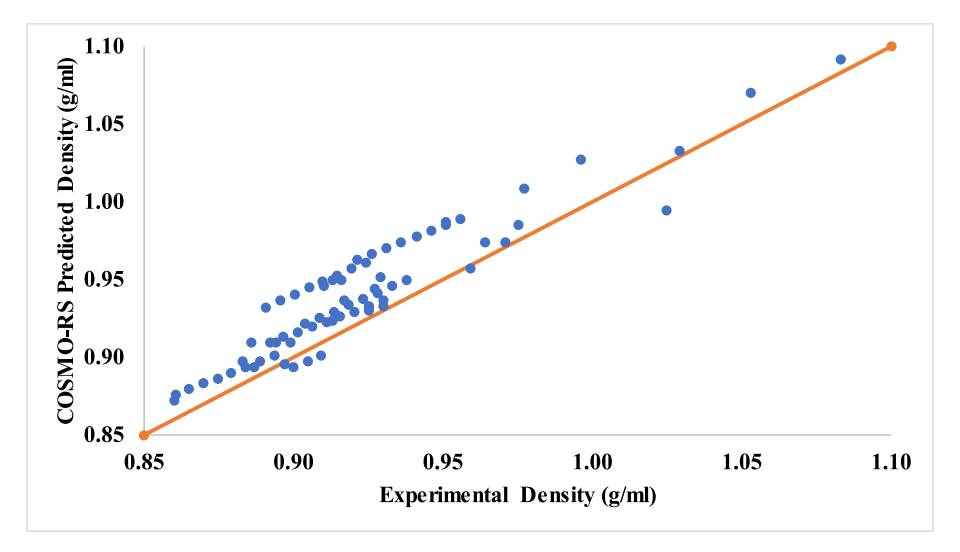


Fig. 1. COSMO-RS Predicted densities for 72 solvents studied in this experiment vs literature values. The close the values are to the orange line of slope 1, the more accurate the predicted value. Each blue dot is a datapoint for (predicted, literature) coordinate. (For interpretation of the references to color in this figure legend, the reader is referred to the web version of this article.)

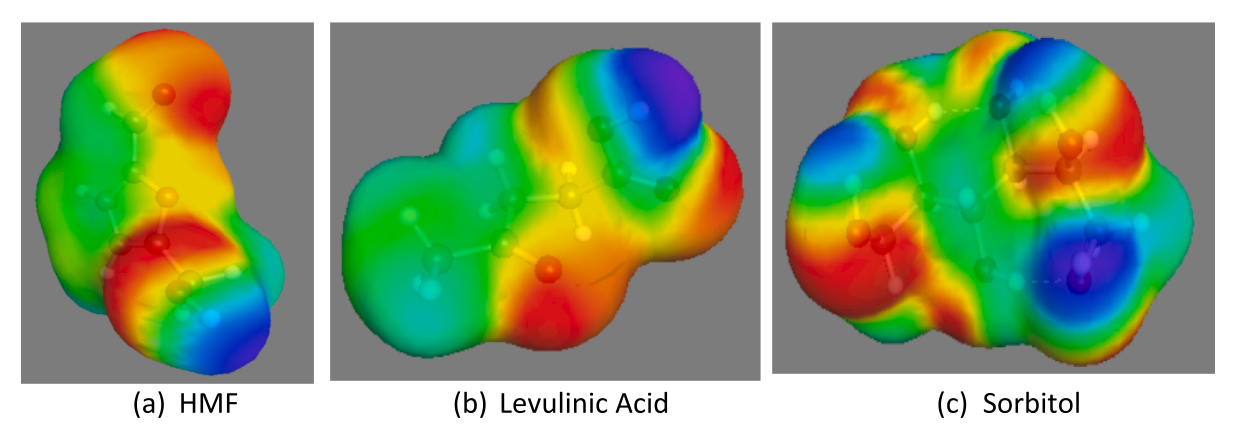


Fig. 2. Sigma surfaces for the three studied platform chemicals in this research as generated by TmoleX. Red indicates electron dense regions, blue to electron deficient regions, and green to electron neutral regions. (For interpretation of the references to color in this figure legend, the reader is referred to the web version of this article.)

reserved for unstable molecules.

Sigma profiles are histograms of 2-dimensional compressions of the 3-dimensional generated sigma surfaces of molecules [34]. Integrating the sigma profile results in the total sigma surface area of the molecule it represents. There are three segments of a sigma plot that represent hydrogen bonding donating, hydrogen bond accepting, and van der Waals interactions [34]. Curves that contain area between the x-axis values of \pm 0.0079 $e/\text{Å}^2$ represent sigma surfaces available for van der Waals interactions with adjacent molecules. Curvature area below $-0.0079 \, e/\text{Å}^2$ represents the amount of molecular surface available for hydrogen bond donating interactions. Meanwhile, curvature area above $0.0079 \ e/\text{Å}^2$ represents the amount of molecular surface available for hydrogen bond accepting interactions. From Fig. 3a, the sigma profiles of sorbitol, HMF, and levulinic acid show most of the curvature area being concentrated within the van der Waals interaction region, significant area in the hydrogen bond accepting region, and still significant but relatively small area in the hydrogen bond donating region. Levulinic acid and HMF have almost identical surface charge distributions with $\sim 20\%$ available for hydrogen bond donating, $\sim 42\%$ available for van der Waals interactions, and ~ 38% available for hydrogen bond accepting. Sorbitol trades a significant amount of van der Waals area for hydrogen bond donating with a distribution of 24%, 35%, and 40%,

respectively. The distributions suggest these PC's might be soluble in most solvents due to the polar and non-polar interactions sites. These distributions are not the same for water, which has most of its area divided between the hydrogen bonding zones as expected, alluding to its polar nature. These distributions can be qualitatively witnessed in the color apportioning of the sigma surfaces seen in Fig. 2.

Symmetry around the axis of x = 0 suggests stability for a molecule, whereas asymmetry would lead to an increase in pure compound volatility. All molecules represented are asymmetric except for water. When considering HDES's capability for sorbitol, HMF, or levulinic acid, an ideal sigma profile pairing would be one of a mirror-image where asymmetric solvents would be balanced by their asymmetric solute counterpart, and symmetry within the van der Waals region for both PC and HDES would produce a stable mixture. Qualitatively according to Fig. 3a, it would appear the rank in order of most volatile to least PC would be levulinic acid > HMF > sorbitol, this is confirmed quantitatively by their melting points of \sim 33 °C, \sim 35 °C, and \sim 100 °C, respectively [37-39]. Regarding the sigma profiles found in Fig. 3b, two representative HBAs (N4Br and menthol) and selected HBDs, all molecules show a shift of their peaks to the negative values rather than at zero within the van der Waals region. While their area remains in the van der Waals region, they may be influenced by polar PCs to partake in low energy hydrogen bonding, dependent upon how close this peak is to the

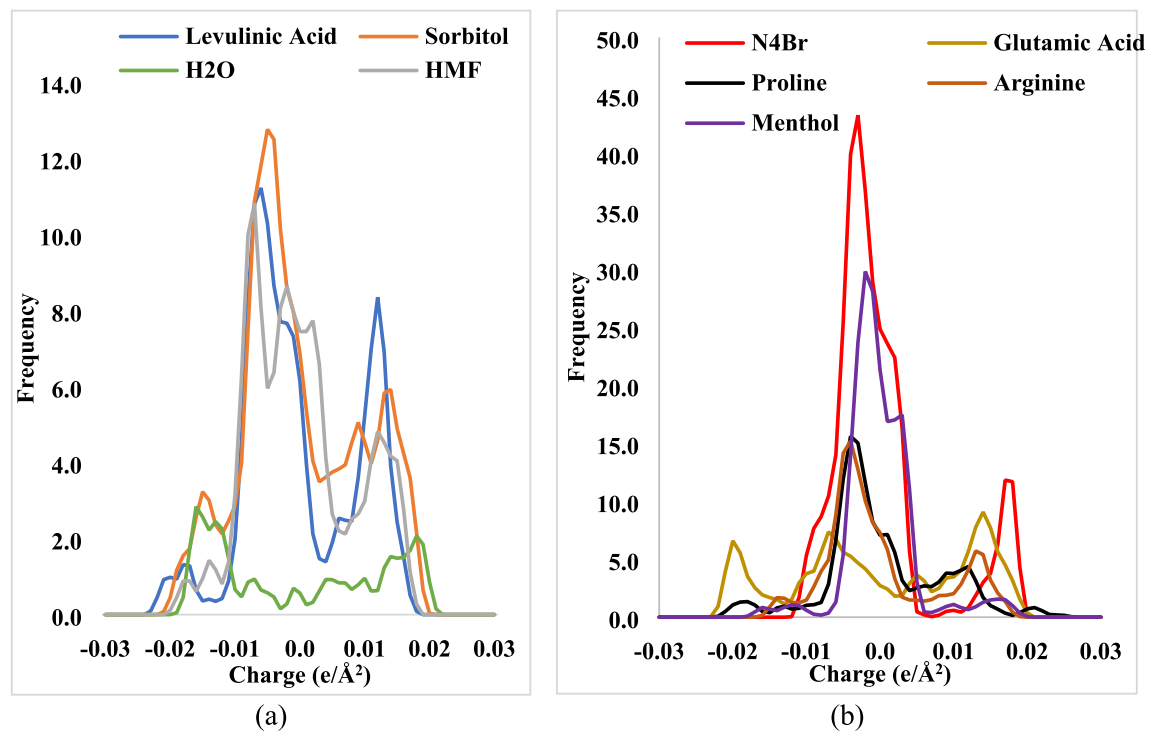


Fig. 3. A: sigma profiles of the three pc analytes and water as a reference. y-axis is frequency, x-axis is charge per angstrom squared. Fig. 3b: Sigma profiles as predicted by TmoleX for the top 3 performing solvents HBA and HBD components. All three solvents were comprised of the N4Br HBA, the other3 components are HBD. The y axis scales are made dissimilar for resolution.

border regions. Similar phenomenon was seen for CO_2 which can be absorbed by both polar and non-polar solvents even though its naturally a non-polar molecule [21]. The HDES show similarity between peak location and area distribution; thus, any solute interaction difference will be likely due to the minor shifts in these properties towards or away from the hydrogen donating region.

The sigma potential plots offer a quantitative analysis of how a molecule will behave in a certain electrostatic environment (Fig. 4). While sigma profile allows comparison of the molecular surface charges, the sigma potential plots compare the entire molecule's chemical potential in response to a specifically charged surface. The x-axis of sigma potential plot is the charge ranging the same scale as the sigma profile $(\pm 0.03 \text{ e/Å}^2)$. The y-axis is the chemical potential of the solute molecule

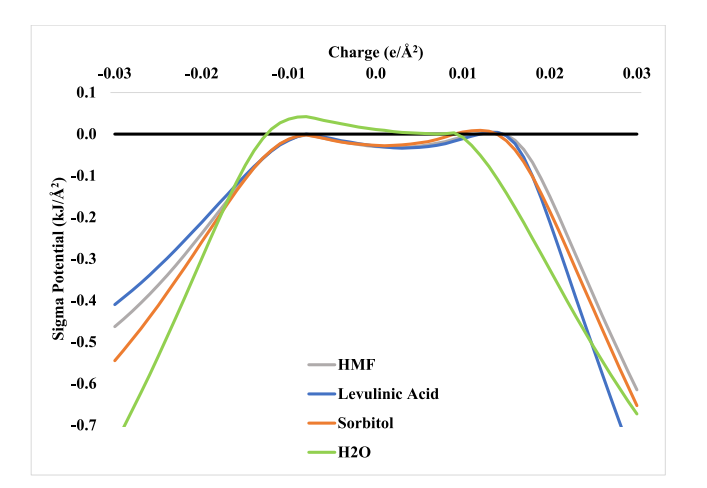


Fig. 4. Sigma potentials as calculated by TmoleX for the three studied PC's and water as a reference. The x-axis is the same as the profiles, but the y-axis represents chemical potential instead of frequency of occurrence for a given x-value.

in the charged solvent environment. Chemical potential with positive values indicates non-spontaneous interactions, or repulsive effects. Chemical potentials with negative values indicate spontaneous molecular interactions, or attractive effects. Considering the sigma potential curves for water and PCs in Fig. 4, several details about the PCs may be obtained regarding separations from aqueous solution. First, there is an overlay effect occurring between the PCs and the water as they share curve characteristics, which suggests they are soluble in aqueous solutions. The relatively slow incremental sloping of the water curve around -0.01 e/Å^2 , along with the almost linear behavior suggest strong dielectric characteristics [34]. This corresponds well with the sigma profile of water (Fig. 3a) which has a symmetrical distribution of area between the hydrogen bonding regions. A similar behavior can be seen in Fig. 4 for the PCs, which lends to the broad distribution of surface charge range for each seen in Fig. 3a. The van der Waals region of the sigma potential plots indicates the relative hydrophobicity of a molecule, curves that drop below those of water in this region are considered increasingly hydrophobic with decrease in value. It can be seen from Fig. 4, all PC's behave similarly with this respect and do not drop significantly below zero, suggesting water solubility but not hydrophilicity. This behavior insight corresponds to the significant amount of surface charge area with near neutral charge each PC possesses. Since roughly 30% of their area is in the hydrogen bond accepting region and the bulk in van der Waals ($\pm 0.0079 \text{ e/Å}^2$), it is expected for HDES that have high amounts of area concentrated between the hydrogen donating and van der Waals regions (near -0.0079 e/Å^2), to offer the better absorption.

3.3. COSMO-RS screening of HDES

In this COSMO-RS screening, activity coefficients of sorbitol, HMF, and levulinic acid in each of the 105 HDES were calculated at standard temperature and pressure. These conditions were chosen as all HDES are reported to be liquid below room temperature [23]. Also, both HDES

and PCs are incompressible with low volatility. The activity coefficient was chosen as the screening parameter as this is also directly related to solubility [40,41,42]. Fig. 5 is a radar plot of the activity coefficients for each PC and water in each HDES. Each HDES is identifiable by keeping the numbering same as Table 1. Values of ln $(\gamma) = 1$ follow the ideal Raoults law, where values above and below one require the modified version that considers non-ideality. Any ln (γ) values above one indicates repulsive electrostatic interactions between HDES-PC combinations. ln $(\gamma) < 1$ indicates attractive electrostatic interactions. Thus, any values that fall outside of the limited r-axis are screened out from Fig. 5.

One of the notable features of Fig. 5 is the "hydrophobicity" of the HDES. While considered hydrophobic by literature, nearly all solvents show slight hydrophilicity (1 > $\ln \gamma \le 0$) to moderate hydrophilicity (0 > $ln\gamma \leq 2$). According to the ranked HDES from Fig. 5, the three HDES possessing the highest solubilization power for all three PC's is N4Br combined with L-arginine > L-proline > L-glutamic acid ranked in order from best to worst performing of the three. To determine the mechanisms of solvation one must revisit Fig. 3a, Fig. 3b, and Fig. 4. Glutamic acid, which was ranked third, has three distinct peaks in the strong hydrogen bonding donating region, hydrogen bond accepting region, and van der Waals interactions zone. This profile suggests glutamic acid is the most versatile HBD regarding these amino acids. However, more sigma surface area of PCs favors van der Waals interactions over either hydrogen bonding type. This is likely the factor which allows proline and arginine to outperform glutamic acid, as they have significantly more sigma surface area distributed in the van der Waals region. It can be qualitatively deduced through Fig. 3 that a high similarity between the area distributions of the PCs and arginine, proline, and N4Br exists.

Since both PCs and HDES are considered stable in their pure forms and complement each other's sigma distribution, it is reasonable to conclude that they would form strong stable structures with each other when mixed. The culmination of these factors results in the high solubility these PC's experience with these three HDES. These HDES have significant amounts of van der Waals interactions surface, strong hydrogen bond accepting surface, and electrostatically moderate to strong hydrogen bond donating surface. As previously discussed, the molecules of HMF and levulinic acid offer nearly identical charge distributions while sorbitol deviates from the group in this respect. This observation coincides with the $\sim 2x$ or more activity coefficients for sorbitol compared to either HMF or levulinic acid observed in Fig. 5. Meanwhile, three HDES with the least solvation power for PC's are detailed and contrasted by the three top performing solvents in Fig. 6 by presenting their computed ln activity coefficients. On the basis of favorable electrostatic interactions, it can be seen in Fig. 3b that menthol does not meet the requirements, resulting in high $ln(\gamma)$. Menthol concentrates nearly all its surface charge in the central van der Waals region. In contrast, N4Br has a much larger distribution of surface charge. This characteristic becomes a repulsive trait when interacting with the highly non-polar terpene based HBA's like menthol and thymol. Thus, resulting in poor solubilization.

3.4. Excess enthalpy of PC's in HDES

The total excess enthalpy of interaction (H_{int}) computed by COSMO-RS is comprised of enthalpy change due to hydrogen bonding (H_{hb}), change due to van der Waals interactions (H_{vdw}), and misfit energy (H_{mt})

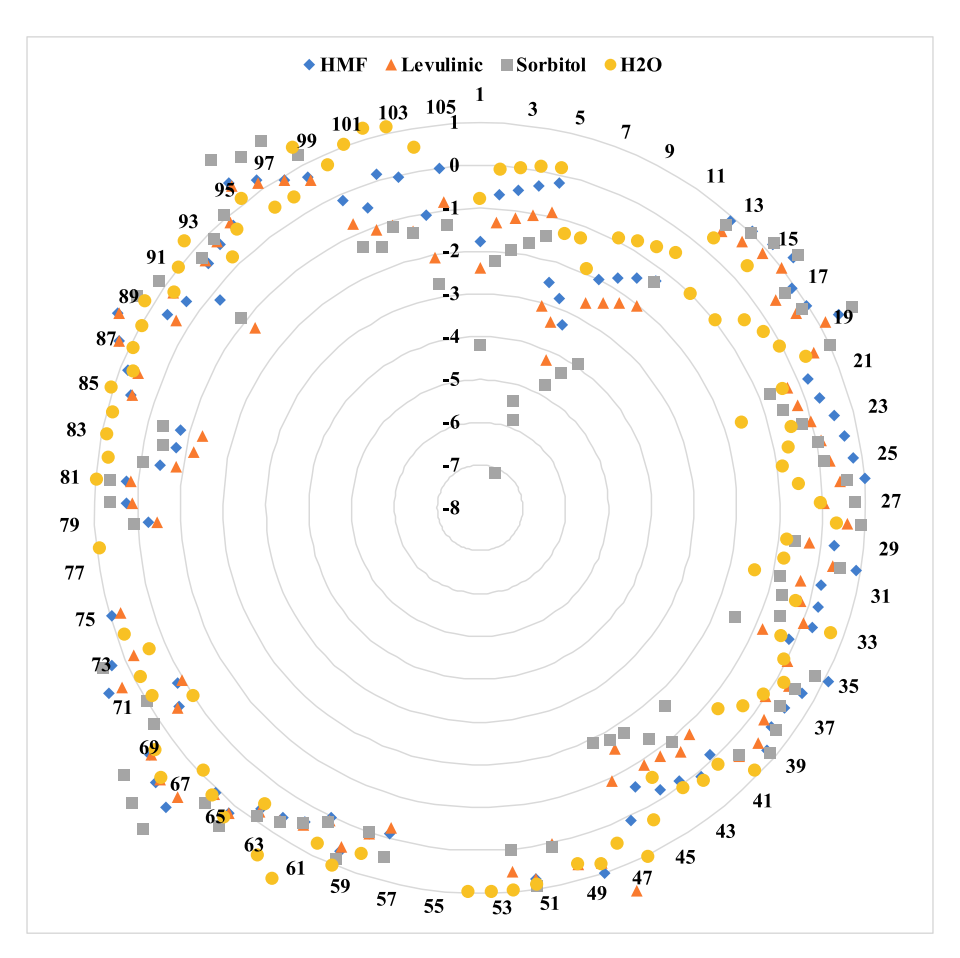


Fig. 5. Radar plot of ln activity coefficients for all studied solvent–solute systems. Values closest to the center represent solvents that have a higher affinity for the given solute than the points with increasing distance from center. The point is related to the solvent name on the outer rim of the radar radially in the vector from center.

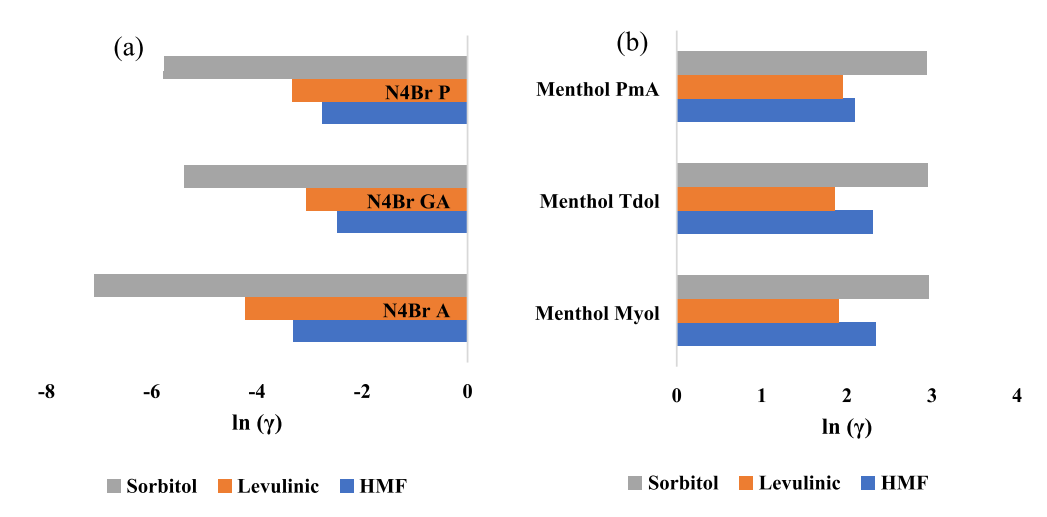


Fig. 6. Predicted In activity coefficients of top five performing solvents for solubilizing PC's (A). Predicted In activity coefficients for bottom five performing solvents for PC solubilization. The more positive values equal less affinity between solvent–solute. Even the five worst performing HDES suggest higher affinity for PC's than convention.

Table 2
Enthalpic values per contribution term for all three solutes in 5 top performing solvents. These solvents are as follows: Tetrabutylammonium bromide with acetic acid (N4Br AA), Tetrabutylammonium bromide with glutamic acid (N4Br GA), Tetrabutylammonium bromide with l-proline (N4Br P), Tetrabutylammonium bromide with l-arginine (N4Br A), and Tetrabutylammonium bromide with 1-butanol (N4Br Bol). All values have units of kJ/mol.

	НМБ			Levulinic Acid		Sorbitol			
	H _{mf} (kJ/mol)	H _{HB} (kJ/mol)	H _{VdW} (kJ/mol)	H _{mf} (kJ/mol)	H _{HB} (kJ/mol)	H _{VdW} (kJ/mol)	H _{mf} (kJ/mol)	H _{HB} (kJ/mol)	H _{VdW} (kJ/mol)
N4Br AA	3.70	-3.91	-7.54	3.73	-4.64	-7.27	3.98	-9.38	-9.16
N4Br GA	3.90	-3.87	-7.65	3.93	-4.65	-7.39	4.18	-9.35	-9.31
N4Br P	3.95	-3.86	-7.67	3.98	-4.67	-7.40	4.24	-9.36	-9.33
N4Br A	4.03	-4.94	-7.66	4.07	-6.40	-7.38	4.39	-11.9	-9.29
N4Br Bol	3.78	-3.95	-7.62	3.81	-4.70	-7.36	4.06	-9.50	-9.28

(Table 2). Fig. 7 contains the enthalpies calculated for each PC for each of the top three HDES. The total excess enthalpy of interaction (H_{int}) values are all negative as solvating the PCs is an exothermic and spontaneous occurrence. This is consistent with the radar plot described ln (γ). A familiar trend appears as the H_{int} values for HMF, levulinic acid,

and sorbitol increase in this respective order with the solubilization (Fig. 6). Other observations include the consistent values for H_{mf} , relatively consistent H_{vdw} values compared to changes in H_{HB} , and the difference of H_{int} values for each solvent-PC combination being driven by changes in H_{HB} . The expressed consistency of the H_{MF} values is likely due

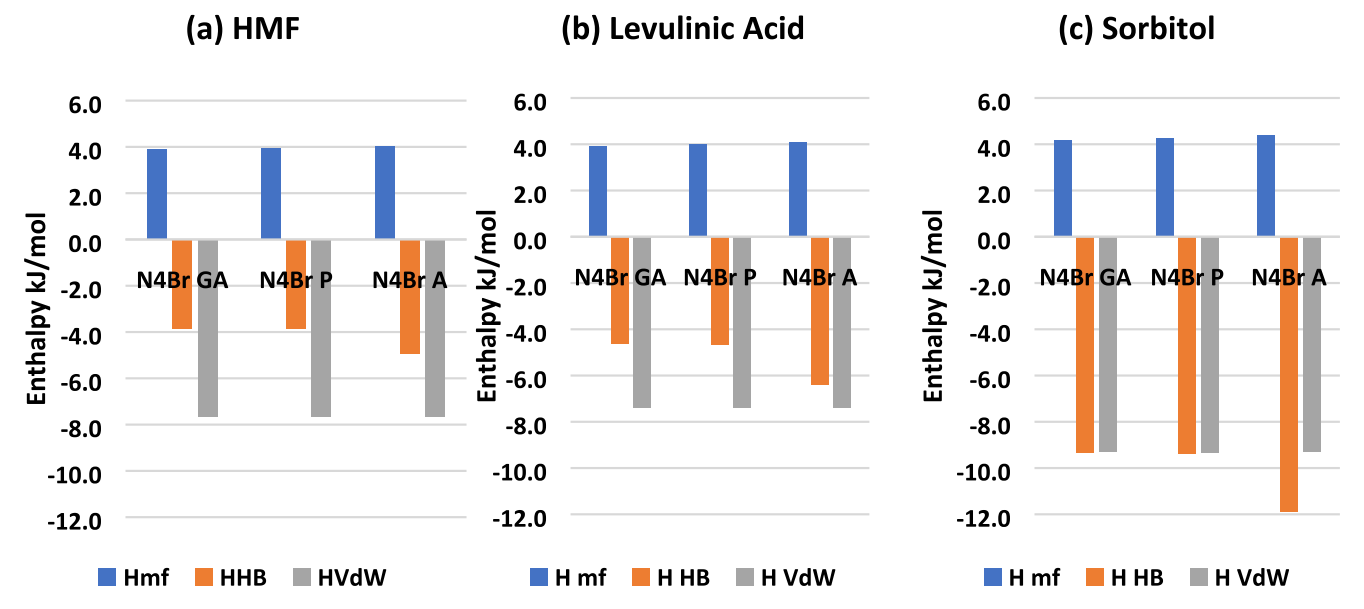


Fig. 7. Excess enthalpies per contribution term per solvent for HMF(A), Levulinic Acid (B), and Sorbitol (C). The total excess enthalpy for a solvent–solute mixture is the sum of the three parameters depicted. Positive values equate to endothermic processes and negative to exothermic processes, which would occur spontaneously. N4Br:A would have the highest total excess enthalpy.

to the similarity between HDES and PCs respective sizes and surface profiles, since the main contributor to changes in H_{mf} are from surface charge mismatch and steric hindrance [34]. The discrepancy between H_{vdw} and H_{HB} values for sorbitol compared to HMF and levulinic acid are explained through the sigma surface charge distributions, which were nearly identical for HMF and levulinic acid, but sorbitol had more hydrogen bonding area than exchanged neutral surface charge area. Therefore, more enthalpically favorable charge matches for the H_{HB} term are likely to exist, resulting in more negative H_{HB} values for sorbitol and similar ones for HMF and levulinic acid. The final observation is N4Br:A consistently expressing the most negative H_{HB} values of the three down selected solvents, despite its strikingly similar charge distribution profile to N4Br:P (seen in Fig. 3b). While there is a favorable slight shift of the van der Waals region peak towards the charge deficiency region for N4Br:A compared to N4Br:P, the main difference in the performance of the two likely resides in the composition of the two solvents. N4Br:A has a composition of 8:1 while N4Br:P has a composition of 4:1. The larger mass of N4Br:A equates to an increase in sigma surface interaction sites. A similar finding from McGaughy et al [12] regarding HDES and the platform chemical furfural suggests that among near identical solvent components for HDES, the attribute of the solvent to contain specific favorable interactions sites does not guarantee optimal interactions but rather the ratio of these surface charges to one another. Using the same HBD and five varying chain lengths of alkyl ammonium bromide their finding was the middle alkyl chain length being hexa ammonium bromide outperforming the others. It is evident that the ability for N4Br and three amino acid HBDs to solvate PCs comes from its ability to form a complimentary hydrogen bonding-van der Waals interaction complex.

4. Conclusions

This study has provided significant insight into the electrostatic solubilization mechanisms associated with 105 HDES on HMF, levulinic acid, and sorbitol. Through generation of the sigma profiles and sigma potential plots for each platform chemical, it was shown that HDES with more van der Waals interaction sites along with moderate hydrogen bonding regions offer the best solubilization potential. This resulted in the down-selection of the HBA N4Br, with three different amino acids (arginine, glutamic acid, and proline) for HBD as the top three potential HDES for solubilizing platform chemicals. Combining the results of the excess enthalpy parameters H_{mf} , H_{hb} , and H_{vdw} , these HDES could make hydrogen bonding-van der Waals interaction with platform chemicals with negative total excess enthalpy.

CRediT authorship contribution statement

Thomas Quaid: Conceptualization, Investigation, Methodology, Data curation, Formal analysis, Validation. **Toufiq Reza:** Conceptualization, Supervision, Visualization.

Declaration of Competing Interest

The authors declare that they have no known competing financial interests or personal relationships that could have appeared to influence the work reported in this paper.

Data availability

Data will be made available on request.

Acknowledgement

This work was funded through the Petroleum Research Fund by the American Chemical Society (PRF # 60342-DNI9) and by the National Science Foundation under Grant No. 2123495.

Appendix A. Supplementary material

Supplementary data to this article can be found online at https://doi.org/10.1016/j.molliq.2023.121918.

References

- S. Takkellapati, T. Li, M.A. Gonzalez, An Overview of Biorefinery Derived Platform Chemicals from a Cellulose and Hemicellulose Biorefinery, Clean Technol. Environ. Policy 20 (7) (Sep. 2018) 1615–1630, https://doi.org/10.1007/s10098-018-1568-5
- [2] T. Werpy, G. Petersen, Top Value Added Chemicals from Biomass: Volume I Results of Screening for Potential Candidates from Sugars and Synthesis Gas, National Renewable Energy Lab., Golden, CO (US), DOE/GO-102004-1992, Aug. 2004. doi: 10.2172/15008859.
- [3] C.-W. Chiu, M.A. Dasari, G.J. Suppes, W.R. Sutterlin, Dehydration of glycerol to acetol via catalytic reactive distillation, AIChE J. 52 (10) (2006) 3543–3548, https://doi.org/10.1002/aic.10951.
- [4] C.H.J.T. Dietz, F. Gallucci, M. Van Sint Annaland, C. Held, M.C. Kroon, 110th Anniversary: Distribution Coefficients of Furfural and 5-Hydroxymethylfurfural in Hydrophobic Deep Eutectic Solvent + Water Systems: Experiments and Perturbed-Chain Statistical Associating Fluid Theory Predictions, Ind. Eng. Chem. Res. 58 (10) (2019) 4240–4247, https://doi.org/10.1021/acs.iecr.8b06234.
- [5] L.C. Blumenthal, C.M. Jens, J. Ulbrich, F. Schwering, V. Langrehr, T. Turek, U. Kunz, K. Leonhard, R. Palkovits, Systematic Identification of Solvents Optimal for the Extraction of 5-Hydroxymethylfurfural from Aqueous Reactive Solutions, ACS Sustain. Chem. Eng. 4 (1) (2016) 228–235.
- [6] R. Svigelj, N. Dossi, C. Grazioli, R. Toniolo, Deep Eutectic Solvents (DESs) and Their Application in Biosensor Development, Sensors 21 (13) (Jun. 2021) 4263, https://doi.org/10.3390/s21134263.
- [7] B.B. Hansen, S. Spittle, B. Chen, D. Poe, Y. Zhang, J.M. Klein, A. Horton, L. Adhikari, T. Zelovich, B.W. Doherty, B. Gurkan, E.J. Maginn, A. Ragauskas, M. Dadmun, T.A. Zawodzinski, G.A. Baker, M.E. Tuckerman, R.F. Savinell, J. R. Sangoro, Deep Eutectic Solvents: A Review of Fundamentals and Applications, Chem. Rev. 121 (3) (2021) 1232–1285.
- [8] A.P. Abbott, G. Capper, D.L. Davies, R.K. Rasheed, V. Tambyrajah, Novel solvent properties of choline chloride/urea mixtures, Chem. Commun. 1 (Jan. 2003) 70–71, https://doi.org/10.1039/B210714G.
- [9] S. Khandelwal, Y.K. Tailor, M. Kumar, Deep eutectic solvents (DESs) as eco-friendly and sustainable solvent/catalyst systems in organic transformations, J. Mol. Liq. 215 (Mar. 2016) 345–386, https://doi.org/10.1016/j.molliq.2015.12.015.
- [10] A.K. Halder, M.N.D.S. Cordeiro, Probing the Environmental Toxicity of Deep Eutectic Solvents and Their Components: An In Silico Modeling Approach, ACS Sustain. Chem. Eng. 7 (12) (Jun. 2019) 10649–10660, https://doi.org/10.1021/ acssuschemeng.9b01306.
- [11] A. Shishov, A. Bulatov, M. Locatelli, S. Carradori, V. Andruch, Application of deep eutectic solvents in analytical chemistry. A review, Microchem. J. 135 (Nov. 2017) 33–38, https://doi.org/10.1016/j.microc.2017.07.015.
- [12] K. McGaughy, M.T. Reza, Liquid–Liquid Extraction of Furfural from Water by Hydrophobic Deep Eutectic Solvents: Improvement of Density Function Theory Modeling with Experimental Validations, ACS Omega 5 (35) (Sep. 2020) 22305–22313, https://doi.org/10.1021/acsomega.0c02665.
- [13] "Rodriguez: Aliphatic–aromatic separation using... Google Scholar." https://scholar.google.com/scholar_lookup?hl=en&volume=54&publication_year=2015&pages=11404-11412&author=N.+R.+Rodriguezauthor=P.+F.+Requejoauthor=M.+C.+Kroon&title=Aliphatic%E2%80%93Aromatic+Separation+Using+Deep+Eutectic+Solvents+as+Extracting+Agents&doi=10.1021%2Facs.iecr.5b02611 (accessed Jun. 26, 2022).
- [14] F.S. Oliveira, A.B. Pereiro, L.P.N. Rebelo, I.M. Marrucho, Deep eutectic solvents as extraction media for azeotropic mixtures, Green Chem. 15 (5) (Apr. 2013) 1326–1330, https://doi.org/10.1039/C3GC37030E.
- [15] P. Makoś, E. Stupek, J. Gębicki, Extractive detoxification of feedstocks for the production of biofuels using new hydrophobic deep eutectic solvents – Experimental and theoretical studies, J. Mol. Liq. 308 (Jun. 2020), 113101, https://doi.org/10.1016/j.molliq.2020.113101.
- [16] A.P. Abbott, G. Capper, D.L. Davies, K.J. McKenzie, S.U. Obi, Solubility of Metal Oxides in Deep Eutectic Solvents Based on Choline Chloride, J. Chem. Eng. Data 51 (4) (Jul. 2006) 1280–1282, https://doi.org/10.1021/je060038c.
- [17] D.J.G.P. van Osch, L.F. Zubeir, A. van den Bruinhorst, M.A.A. Rocha, M.C. Kroon, Hydrophobic deep eutectic solvents as water-immiscible extractants, Green Chem. 17 (9) (Sep. 2015) 4518–4521, https://doi.org/10.1039/C5GC01451D.
- [18] M. Tiecco, F. Cappellini, F. Nicoletti, T. Del Giacco, R. Germani, P. Di Profio, Role of the hydrogen bond donor component for a proper development of novel hydrophobic deep eutectic solvents, J. Mol. Liq. 281 (May 2019) 423–430, https:// doi.org/10.1016/j.molliq.2019.02.107.
- [19] A.K. Dwamena, Recent Advances in Hydrophobic Deep Eutectic Solvents for Extraction, Separations 6 (1) (Feb. 2019) 9, https://doi.org/10.3390/ separations6010009.
- [20] M.A.R. Martins, E.A. Crespo, P.V.A. Pontes, L.P. Silva, M. Bülow, G.J. Maximo, E.A. C. Batista, C. Held, S.P. Pinho, J.A.P. Coutinho, Tunable Hydrophobic Eutectic Solvents Based on Terpenes and Monocarboxylic Acids, ACS Sustain. Chem. Eng. 6 (7) (2018) 8836–8846.

- [21] T. Quaid, M.T. Reza, Carbon Capture from Biogas by Deep Eutectic Solvents: A COSMO Study to Evaluate the Effect of Impurities on Solubility and Selectivity, Clean Technol. 3 (2) (Jun. 2021) 490–502.
- [22] A.K. Dwamena, D.E. Raynie, Solvatochromic Parameters of Deep Eutectic Solvents: Effect of Different Carboxylic Acids as Hydrogen Bond Donor, J. Chem. Eng. Data 65 (2) (Feb. 2020) 640–646, https://doi.org/10.1021/acs.jced.9b00872.
- [23] D.J.G.P. van Osch, C.H.J.T. Dietz, S.E.E. Warrag, M.C. Kroon, The Curious Case of Hydrophobic Deep Eutectic Solvents: A Story on the Discovery, Design, and Applications, ACS Sustain. Chem. Eng. 8 (29) (Jul. 2020) 10591–10612, https://doi.org/10.1021/acssuschemeng.0c00559.
- [24] W. Deng, L. Yu, X. Li, J. Chen, X. Wang, Z. Deng, Y. Xiao, Hexafluoroisopropanol-based hydrophobic deep eutectic solvents for dispersive liquid-liquid microextraction of pyrethroids in tea beverages and fruit juices, Food Chem. 274 (2019) 891–899.
- [25] F. Eckert, A. Klamt, Fast solvent screening via quantum chemistry: COSMO-RS approach, AIChE J. 48 (2) (2002) 369–385, https://doi.org/10.1002/aic.690480220
- [26] L. Jiřiště, M. Klajmon, Predicting the Thermodynamics of Ionic Liquids: What to Expect from PC-SAFT and COSMO-RS? J. Phys. Chem. B 126 (20) (May 2022) 3717–3736, https://doi.org/10.1021/acs.jpcb.2c00685.
- [27] I. Adeyemi, R. Sulaiman, M. Almazroui, A. Al-Hammadi, I.M. AlNashef, Removal of chlorophenols from aqueous media with hydrophobic deep eutectic solvents: Experimental study and COSMO RS evaluation, J. Mol. Liq. 311 (Aug. 2020), 113180, https://doi.org/10.1016/j.molliq.2020.113180.
- [28] A. Cañada-Barcala, D. Rodríguez-Llorente, L. López, P. Navarro, E. Hernández, V. I. Águeda, S. Álvarez-Torrellas, J.C. Parajó, S. Rivas, M. Larriba, Sustainable Production of Furfural in Biphasic Reactors Using Terpenoids and Hydrophobic Eutectic Solvents, ACS Sustain. Chem. Eng. 9 (30) (2021) 10266–10275.
- [29] "TURBOMOLE Documentation & How To," TURBOMOLE. https://www.turbomole.org/turbomole/turbomole-documentation/ (accessed Jun. 26, 2022).
- [30] L.P. Silva, L. Fernandez, J.H.F. Conceição, M.A.R. Martins, A. Sosa, J. Ortega, S. P. Pinho, J.A.P. Coutinho, Design and Characterization of Sugar-Based Deep Eutectic Solvents Using Conductor-like Screening Model for Real Solvents, ACS Sustain. Chem. Eng. 6 (8) (2018) 10724–10734.
- [31] J. Wang, Y. Guo, F. Liu, X. Zhang, W. Wang, Q. Peng, COSMO-RS prediction and experimental verification of deep eutectic solvents for water insoluble pesticides with high solubility, J. Mol. Liq. 349 (Mar. 2022), 118139, https://doi.org/ 10.1016/j.mollin.2021.118139.
- [32] T. Jeliński, P. Cysewski, Application of a computational model of natural deep eutectic solvents utilizing the COSMO-RS approach for screening of solvents with high solubility of rutin, J. Mol. Model. 24 (7) (2018) 01, https://doi.org/10.1007/ s00894-018-3700-1.
- [33] A.S. Darwish, et al., Multicomponent extraction of aromatics and heteroaromatics from diesel using acidic eutectic solvents: Experimental and COSMO-RS predictions, J. Mol. Liq., vol. 336, p. 116575, Aug. 2021, doi: 10.1016/j. molliq.2021.116575.
- [34] K.N. Marsh, "COSMO-RS from Quantum Chemistry to Fluid Phase Thermodynamics and Drug Design. By A. Klamt. Elsevier: Amsterdam, The Netherlands, 2005. 246 pp. \$US 165. ISBN 0-444-51994-7., J. Chem. Eng. Data, vol. 51, no. 4, pp. 1480–1480, Jul. 2006, doi: 10.1021/je0602317.
- [35] T. Lemaoui, A.S. Darwish, N.E.H. Hammoudi, F. Abu Hatab, A. Attoui, I. M. Alnashef, Y. Benguerba, Prediction of Electrical Conductivity of Deep Eutectic Solvents Using COSMO-RS Sigma Profiles as Molecular Descriptors: A Quantitative Structure-Property Relationship Study, Ind. Eng. Chem. Res. 59 (29) (2020) 13343–13354.
- [36] L. Sellaoui, G.L. Dotto, E.C. Peres, Y. Benguerba, É.C. Lima, A.B. Lamine, A. Erto, New insights into the adsorption of crystal violet dye on functionalized multiwalled carbon nanotubes: Experiments, statistical physics and COSMO–RS models application, J. Mol. Liq. 248 (2017) 890–897.
- [37] PubChem, "Sorbitol." https://pubchem.ncbi.nlm.nih.gov/compound/5780 (accessed Jun. 25, 2022).
- [38] PubChem, "Levulinic acid." https://pubchem.ncbi.nlm.nih.gov/compound/11579 (accessed Jun. 25, 2022).
- [39] "5-(Hydroxymethyl)furfural analytical standard 67-47-0." http://www.sigmaaldrich.com/ (accessed Jun. 25, 2022).
- [40] T. Brouwer, S.R.A. Kersten, G. Bargeman, B. Schuur, trends in solvent impact on infinite dilution activity coefficients of solutes reviewed and visualized using an algorithm to support selection of solvents for greener fluid separations, Sep. Purif. Technol. 272 (Oct. 2021), 118727, https://doi.org/10.1016/j. seppur.2021.118727.
- [41] K.A. Kurnia, S.P. Pinho, J.A.P. Coutinho, Evaluation of the Conductor-like Screening Model for Real Solvents for the Prediction of the Water Activity Coefficient at Infinite Dilution in Ionic Liquids, Ind. Eng. Chem. Res. 53 (31) (Aug. 2014) 12466–12475, https://doi.org/10.1021/ie5021415.
- [42] J. Zhao, G. Zhou, T. Fang, S. Ying, X. Liu, Screening ionic liquids for dissolving hemicellulose by COSMO-RS based on the selective model, RSC Adv. 12 (26) (2022) 16517–16529.
- [43] C. Florindo, L.C. Branco, I.M. Marrucho, Development of hydrophobic deep eutectic solvents for extraction of pesticides from aqueous environments, Fluid Phase Equilibria 448 (Sep. 2017) 135–142, https://doi.org/10.1016/j. fluid.2017.04.002.
- [44] D. Ge, Y. Zhang, Y. Dai, S. Yang, Air-assisted dispersive liquid-liquid microextraction based on a new hydrophobic deep eutectic solvent for the preconcentration of benzophenone-type UV filters from aqueous samples, J. Sep. Sci. 41 (7) (2018) 1635–1643, https://doi.org/10.1002/jssc.201701282.

- [45] C.R. Wright, L. VandenElzen, T.A. Hopkins, Deep Eutectic Solvents for Induced Circularly Polarized Luminescence, J. Phys. Chem. B 122 (37) (Sep. 2018) 8730–8737, https://doi.org/10.1021/acs.jpcb.8b06148.
- [46] W. Tang, Y. Dai, K.H. Row, Evaluation of fatty acid/alcohol-based hydrophobic deep eutectic solvents as media for extracting antibiotics from environmental water, Anal. Bioanal. Chem. 410 (28) (Nov. 2018) 7325–7336, https://doi.org/ 10.1007/s00216-018-1346-6.
- [47] J. Cao, M. Yang, F. Cao, J. Wang, E. Su, Tailor-made hydrophobic deep eutectic solvents for cleaner extraction of polyprenyl acetates from Ginkgo biloba leaves, J. Clean. Prod. 152 (May 2017) 399–405, https://doi.org/10.1016/j. icleana.2017.03.140
- [48] J. Cao, M. Yang, F. Cao, J. Wang, E. Su, Well-Designed Hydrophobic Deep Eutectic Solvents As Green and Efficient Media for the Extraction of Artemisinin from Artemisia annua Leaves, ACS Sustain. Chem. Eng. 5 (4) (Apr. 2017) 3270–3278, https://doi.org/10.1021/acssuschemeng.6b03092.
- [49] K. Zhang, C. Liu, S. Li, J. Fan, A hydrophobic deep eutectic solvent based vortexassisted liquid-liquid microextraction for the determination of formaldehyde from biological and indoor air samples by high performance liquid chromatography, J. Chromatogr. A 1589 (Mar. 2019) 39–46, https://doi.org/10.1016/j. chroma 2018 12 063
- [50] T. Li, Y. Song, J. Xu, J. Fan, A hydrophobic deep eutectic solvent mediated sol-gel coating of solid phase microextraction fiber for determination of toluene, ethylbenzene and o-xylene in water coupled with GC-FID, Talanta 195 (Apr. 2019) 298–305, https://doi.org/10.1016/j.talanta.2018.11.085.
- [51] S. Milker, M. Pätzold, J.Z. Bloh, D. Holtmann, Comparison of deep eutectic solvents and solvent-free reaction conditions for aldol production, Mol. Catal. 466 (Apr. 2019) 70–74, https://doi.org/10.1016/j.mcat.2019.01.012.
- [52] T.E. Phelps, N. Bhawawet, S.S. Jurisson, G.A. Baker, Efficient and Selective Extraction of 99mTc04- from Aqueous Media Using Hydrophobic Deep Eutectic Solvents, ACS Sustain. Chem. Eng. 6 (11) (Nov. 2018) 13656–13661, https://doi. org/10.1021/acssuschemeng.8b03950.
- [53] A. van den Bruinhorst, S. Raes, S.A. Maesara, M.C. Kroon, A.C.C. Esteves, J. Meuldijk, Hydrophobic eutectic mixtures as volatile fatty acid extractants, Sep. Purif. Technol. 216 (Jun. 2019) 147–157, https://doi.org/10.1016/j. seppur.2018.12.087.
- [54] T. Křížek, M. Bursová, R. Horsley, M. Kuchař, P. Tůma, R. Čabala, T. Hložek, Menthol-based hydrophobic deep eutectic solvents: Towards greener and efficient extraction of phytocannabinoids, J. Clean. Prod. 193 (2018) 391–396.
- [55] B.D. Ribeiro, C. Florindo, L.C. Iff, M.A.Z. Coelho, I.M. Marrucho, Menthol-based Eutectic Mixtures: Hydrophobic Low Viscosity Solvents, ACS Sustain. Chem. Eng. 3 (10) (Oct. 2015) 2469–2477, https://doi.org/10.1021/acssuschemeng.5b00532.
- [56] R. Wang, D. Sun, C. Wang, L. Liu, F. Li, Z. Tan, Biphasic recognition chiral extraction of threonine enantiomers in a two-phase system formed by hydrophobic and hydrophilic deep-eutectic solvents, Sep. Purif. Technol. 215 (May 2019) 102–107, https://doi.org/10.1016/j.seppur.2019.01.022.
- [57] M. Hümmer, S. Kara, A. Liese, I. Huth, J. Schrader, D. Holtmann, Synthesis of (-)-menthol fatty acid esters in and from (-)-menthol and fatty acids – novel concept for lipase catalyzed esterification based on eutectic solvents, Mol. Catal. 458 (Oct. 2018) 67–72, https://doi.org/10.1016/j.mcat.2018.08.003.
- [58] A.R. Zarei, M. Nedaei, S.A. Ghorbanian, Ferrofluid of magnetic clay and menthol based deep eutectic solvent: Application in directly suspended droplet microextraction for enrichment of some emerging contaminant explosives in water and soil samples, J. Chromatogr. A 1553 (Jun. 2018) 32–42, https://doi.org/ 10.1016/j.chroma.2018.04.023.
- [59] C. Florindo, A.J.S. McIntosh, T. Welton, L.C. Branco, I.M. Marrucho, A closer look into deep eutectic solvents: exploring intermolecular interactions using solvatochromic probes, Phys. Chem. Chem. Phys. 20 (1) (Dec. 2017) 206–213, https://doi.org/10.1039/C7CP06471C.
- [60] E.E. Tereshatov, M.Y. Boltoeva, C.M. Folden, First evidence of metal transfer into hydrophobic deep eutectic and low-transition-temperature mixtures: indium extraction from hydrochloric and oxalic acids, Green Chem. 18 (17) (Aug. 2016) 4616–4622, https://doi.org/10.1039/C5GC03080C.
- [61] R. Verma, T. Banerjee, Liquid–Liquid Extraction of Lower Alcohols Using Menthol-Based Hydrophobic Deep Eutectic Solvent: Experiments and COSMO-SAC Predictions, Ind. Eng. Chem. Res. 57 (9) (Mar. 2018) 3371–3381, https://doi.org/10.1021/acs.iecr.7b05270.
- [62] A.Y. Shishov, M.V. Chislov, D.V. Nechaeva, L.N. Moskvin, A.V. Bulatov, A new approach for microextraction of non-steroidal anti-inflammatory drugs from human urine samples based on in-situ deep eutectic mixture formation, J. Mol. Liq. 272 (Dec. 2018) 738–745, https://doi.org/10.1016/j.molliq.2018.10.006.
- [63] D.J.G.P. van Osch, C.H.J.T. Dietz, J. van Spronsen, M.C. Kroon, F. Gallucci, M. van Sint Annaland, R. Tuinier, A Search for Natural Hydrophobic Deep Eutectic Solvents Based on Natural Components, ACS Sustain. Chem. Eng. 7 (3) (2019) 2933–2942.
- [64] M.A.R. Martins, L.P. Silva, N. Schaeffer, D.O. Abranches, G.J. Maximo, S.P. Pinho, J.A.P. Coutinho, Greener Terpene-Terpene Eutectic Mixtures as Hydrophobic Solvents, ACS Sustain. Chem. Eng. 7 (20) (2019) 17414–17423.
- [65] P. Makoś, A. Przyjazny, G. Boczkaj, Hydrophobic deep eutectic solvents as 'green' extraction media for polycyclic aromatic hydrocarbons in aqueous samples, J. Chromatogr. A 1570 (Oct. 2018) 28–37, https://doi.org/10.1016/j.chroma.2018.07.070.
- [66] F. Bezold, M. Minceva, Liquid-liquid equilibria of n-heptane, methanol and deep eutectic solvents composed of carboxylic acid and monocyclic terpenes, Fluid Phase Equilibria 477 (Dec. 2018) 98–106, https://doi.org/10.1016/j. fluid.2018.08.020.

- [67] C. Florindo, L. Romero, I. Rintoul, L.C. Branco, I.M. Marrucho, From Phase Change Materials to Green Solvents: Hydrophobic Low Viscous Fatty Acid-Based Deep Eutectic Solvents, ACS Sustain. Chem. Eng. 6 (3) (Mar. 2018) 3888–3895, https://doi.org/10.1021/acssuschemeng.7b04235.
- [68] M.K. AlOmar, M.A. Alsaadi, M. Hayyan, S. Akib, R.K. Ibrahim, M.A. Hashim, Lead removal from water by choline chloride based deep eutectic solvents
- functionalized carbon nanotubes, J. Mol. Liq. 222 (Oct. 2016) 883–894, https://doi.org/10.1016/j.molliq.2016.07.074.
- [69] M. Rajabi, N. Ghassab, M. Hemmati, A. Asghari, Emulsification microextraction of amphetamine and methamphetamine in complex matrices using an up-to-date generation of eco-friendly and relatively hydrophobic deep eutectic solvent, J. Chromatogr. A 1576 (Nov. 2018) 1–9, https://doi.org/10.1016/j. chroma.2018.07.040.